



Geophysical Research Letters

RESEARCH LETTER

10.1029/2020GL089669

Key Points:

- Tropical cyclones that rapidly intensify tend to have larger ice water content prior to intensification
- Ice water content near the storm center is strongly correlated with the intensification rate
- Rapidly intensifying tropical cyclones tend to have a larger initial intensity than more slowly intensifying storms

Supporting Information:

- Supporting Information S1

Correspondence to:

S.-N. Wu,
sww594@rsmas.miami.edu

Citation:

Wu, S.-N., Soden, B. J., & Alaka, G. J. Jr. (2020). Ice water content as a precursor to tropical cyclone rapid intensification. *Geophysical Research Letters*, 47, e2020GL089669. <https://doi.org/10.1029/2020GL089669>

Received 2 JUL 2020

Accepted 14 OCT 2020

Accepted article online 19 OCT 2020

Ice Water Content as a Precursor to Tropical Cyclone Rapid Intensification

S.-N. Wu¹ , B. J. Soden¹ , and G. J. Alaka Jr²

¹Rosenstiel School of Marine and Atmospheric Science, University of Miami, Miami, FL, USA, ²NOAA/AOML/Hurricane Research Division, Miami, FL, USA

Abstract This study examines how the structure and amount of cloud ice water content are related to rates of tropical cyclone (TC) intensification using CloudSat profiling radar measurements and simulations from the Hurricane Weather Research and Forecasting (HWRF) model. Observational studies have demonstrated the signal of TC intensification in the passive satellite measurements of frozen water concentration. However, the vertical and horizontal resolution of passive satellite observations are limited. CloudSat measurements and HWRF simulations provide high-resolution data sets of ice water content to better understand its relationship with the rate of TC intensification. It is found that rapidly intensifying TCs have larger ice water content compared to TCs with slower intensification rates. Similar results are obtained even after accounting for the effect of initial TC intensity. Such precursors of rapidly intensifying TCs may be used to better understand and improve the prediction of TC intensification.

Plain Language Summary It is difficult to accurately forecast future tropical cyclone intensity. Previous studies have analyzed historical tropical cyclones and built statistical hurricane forecast models to predict their intensity changes. These models are good at predicting whether a hurricane will strengthen or weaken. However, they have trouble predicting how fast a tropical cyclone is going to intensify. To better understand intensification rates for tropical cyclones, we analyzed the relationship between intensification rate and the amount of cloud ice from satellite observations and a forecast model. It was found that tropical cyclones with greater amounts of cloud ice are likely to intensify faster. This result suggested that observations of cloud ice may be used to improve the performance of hurricane forecast models.

1. Introduction

The prediction of tropical cyclone (TC) intensity change has improved significantly in the last two decades due to a better understanding of the mechanisms for TC intensification and advances in numerical models (DeMaria et al., 2014; Simon et al., 2018). However, the predictive skill of intensification rates is limited due, in part, to a lack of observations to identify crucial physical processes that trigger TC rapid intensification (Elsberry et al., 2007; Gall et al., 2013). Observations of processes that regulate the evolution of TC intensity can provide key metrics that serve as predictors for future intensification, and almost all these statistical-dynamical techniques currently use information from geostationary satellites for inner core (Kaplan et al., 2010; Knaff et al., 2005, 2020; Shimada et al., 2018). To better understand such processes, it is important to examine observational data that are associated with the primary energy source for TCs, i.e., latent heat release.

Previous theoretical and modeling studies have suggested that both the magnitude and location of latent heat release are important in regulating the evolution of TC intensity (Hack & Schubert, 1986; Nolan et al., 2007). Rogers et al. (2013) demonstrated that the deep convection within the radius of maximum wind is crucial to triggering rapid intensification, while the location of the radius of maximum wind is difficult to estimate without aircraft data. The convective plumes produce latent heating in the region where heating energy can be transformed effectively into kinetic energy (Nolan et al., 2007). Kelley et al. (2004) and Guimond et al. (2010) suggested that these “hot towers” may play a crucial role in TC intensification. Although previous studies have different perspectives on the role of convection in rapidly intensifying TCs, most emphasize the importance of deep convection in triggering rapid intensification. On the

contrary, some studies argue that an increase in stratiform precipitation is important for rapid intensification and that deep convection is a response to rapid intensification rather than a cause (Fischer et al., 2018; Tao et al., 2017). Either way, the lack of direct observations of latent heat release hinders the use of the relationship between latent heating and TC intensification in predicting future TC intensity.

Theoretically, cloud water condensates can serve as a proxy for latent heat release because they are produced simultaneously in the convective updrafts (Cecil & Zipser, 1999; Yanai et al., 1973). In modeling studies, the magnitude of frozen hydrometeor concentration is found to be highly correlated with the amount of latent heat release (Nolan et al., 2019), implying that observations of cloud water condensate can be used as a proxy for latent heat release in TCs.

Satellite measurements of cloud water condensate have been widely used to investigate precursors to TC intensification. Previous studies used observations from the Tropical Rainfall Measurement Mission and found that rapidly intensifying TCs tend to have a broader area with radar reflectivity greater than 20 dBZ compared to nonrapidly intensifying TCs (Jones et al., 2006; Tao & Jiang, 2015; Zagrodnik & Jiang, 2014). Recent studies used microwave-based observations of frozen hydrometeor concentration to investigate their relationship with TC intensification (Alvey et al., 2015; Fischer et al., 2018; Harnos & Nesbitt, 2016). Harnos and Nesbitt (2016) found that the brightness temperature in 87 GHz channel is colder in intensifying TCs than that in weakening TCs, indicating that intensifying TCs have stronger deep convection than weakening TCs. Fischer et al. (2018) also reached the same conclusion, once the effects of TC intensity were accounted for. However, those satellite measurements only provide poorly resolved information of cloud water condensate in both vertical and horizontal directions. Modeling studies suggested that the location of latent heat release, both radially and vertically, is critical in determining the effectiveness of latent heating on TC intensity (Nolan et al., 2007). Therefore, high-resolution observations of cloud water condensates may better depict the relationship between TC intensity and frozen condensate.

CloudSat measures radar reflectivity and uses the measurements to retrieve the vertical distribution of liquid and frozen cloud condensate, providing high-resolution observational metrics of clouds. As a result, CloudSat observations have been widely used as a guidance to evaluate model simulations and passive satellite retrievals of frozen hydrometeors (Chen et al., 2011; Waliser et al., 2009). The data have also proven to be effective in identifying vertical and horizontal distribution of convection in TCs. Tourville et al. (2015) compiled all CloudSat overpasses that penetrate TCs, creating the CloudSat Tropical Cyclone (CSTC) data set. Using the CSTC data set, Wu and Soden (2017) showed that intensifying TCs have, on average, larger ice water content (IWC) than weakening TCs and that this signature exists up to 24 h prior to an intensity change. As previous studies have found signatures of rapidly intensifying TCs in frozen hydrometeors of microwave measurements, it is of interest to further examine whether such signals of rapidly intensifying TCs also occur in frozen water condensate from CloudSat, which has a finer vertical and horizontal resolution than passive satellite measurements.

Furthermore, it is important to evaluate the relationship between rates of TC intensification and frozen hydrometeors in high-resolution numerical weather prediction models in order to improve the predictive skill and our understanding of critical physical processes responsible for rapid intensification. The Hurricane Weather and Research Forecasting model (HWRF; Atlas et al., 2015; Bao et al., 2012; Gopalakrishnan et al., 2011, 2012, 2013; Mehra et al., 2018; Tallapragada et al., 2014) is one of the top-performing operational hurricane prediction models (Lewis et al., 2020). As HWRF provides high-resolution parameters in space and time, examining the signal of rapidly intensifying TCs in HWRF can provide additional insight into the behavior of the physical processes in rapidly intensifying storms. The Basin-scale HWRF (HWRF-B) was developed at NOAA's Atlantic Oceanographic and Meteorological Laboratory in collaboration with NOAA's Environmental Modeling Center and the Developmental Testbed Center as a parallel project to the operational HWRF (Alaka et al., 2017; Zhang et al., 2016). HWRF-B has a nearly identical configuration to HWRF except for some advanced options that will be discussed in section 2.3.

The goal of this study is to evaluate the relationships between IWC and rapidly intensifying TCs in the CSTC data set and high-resolution HWRF-B forecasts. In section 2, we describe the data and methods. The results are presented in section 3, and the conclusions are shared in section 4.

Table 1

The Number of Overpasses Included in the Analysis as a Function of Storm Category and Future (+24 h) Intensification Rates

Category	Number			
	Weakening (<0 kt)	Neutral (0–4 kt)	Slowly (5–9 kt) intensifying	Rapidly (>30 kt) intensifying
Tropical Depression (<34 kt)	47	47	54	3
Tropical Storm (34–63 kt)	95	27	53	14
Category 1–3 (64–1,112 kt)	73	9	27	9
All categories	215	83	134	26

2. Data and Methods

2.1. CloudSat

The Cloud profiling radar on CloudSat provides high-resolution vertical profiles of cloud IWC with 125 vertical levels and horizontal resolution of 1.1 km (Stephens et al., 2002). CSTC data set includes those CloudSat swaths that are within 1,000 km of the TC center (Tourville et al., 2015). This study adopts the overpasses from the year 2006 to 2015 on a global scale, while 2011–2015 data contain day-time only overpasses. To focus on the TC inner core region, we only select swaths whose distance to the TC center is less than 100 km, with 455 overpasses. In addition, since CloudSat penetrates TCs at varying distance to the TC center, we select the point on the swath that is closest to its TC center and define it as the point of closest approach (PCA) when creating composites of CloudSat swaths. In this study, retrievals of IWC are from the CloudSat Radar-Only Cloud Water Content Product (2B-CWC-RO, P_R04 version). In addition, we also included analysis using IWC from 2C-ICE version which utilized CloudSat and CALIPSO observations for retrievals. More details about the compositing method are provided in Wu and Soden (2017).

2.2. TC Intensity

TC information is from the best track archives from International Best Track Archive for Climate Stewardship (IBTrACS), which provide 6-hourly intensity and track of historical TCs (Knapp et al., 2018). We adopt these best track archives to quantify changes in TC intensity for every selected CloudSat overpass. Because CloudSat overpasses are asynchronous, TC intensity is linearly interpolated to the time of CloudSat overpass. Rates of TC intensification are defined as the difference in TC intensity between the CloudSat overpass time and 24 h later. We separate these overpasses into four groups based on rates of TC intensification over that 24-h period: weakening (less than 0 kt), neutral (0 to less than 5 kt), slowly intensifying (5 to less than 30 kt), and rapidly intensifying (equal or greater than 30 kt) TCs. Table 1 lists the number of cases for each group in CloudSat measurements. The threshold of 30 kts in 24 h for the rapidly intensifying category is consistent with previous work by Kaplan and DeMaria (2003). The results in section 3 are not sensitive to minor changes in the thresholds for each intensification group.

2.3. HWRF-B

The high-resolution HWRF-B system was developed under the auspices of the Hurricane Forecast Improvement Program (Gopalakrishnan et al., 2020). It shares most configuration options with the operational HWRF. HWRF is a triply nested modeling system, with an outermost domain that does not move throughout a forecast to capture the synoptic-scale environment (13.5 km) and two storm-following nested domains (4.5 and 1.5 km, respectively) to resolve clouds and sharp gradients within a TC eyewall and rainbands. HWRF is also configured with an advanced suite of physics parameterizations, including the Ferrier-Aligo microphysics scheme (Ferrier et al., 2002; Rogers et al., 2001), the Scale-Aware Simplified Arakawa-Schubert (SASAS) cumulus parameterization scheme (Arakawa & Schubert, 1974; Grell, 1993; Pan & Wu, 1995), and the RRTMG longwave and shortwave radiation schemes (Iacono et al., 2008; Mlawer et al., 1997). For more information about the HWRF system, such as additional parameterizations, refer to the documentation (Biswas et al., 2018).

HWRF-B has a nearly identical configuration to HWRF plus two advanced options not available in the operational HWRF: (i) a large, static outermost domain that spans the entire area of responsibility of

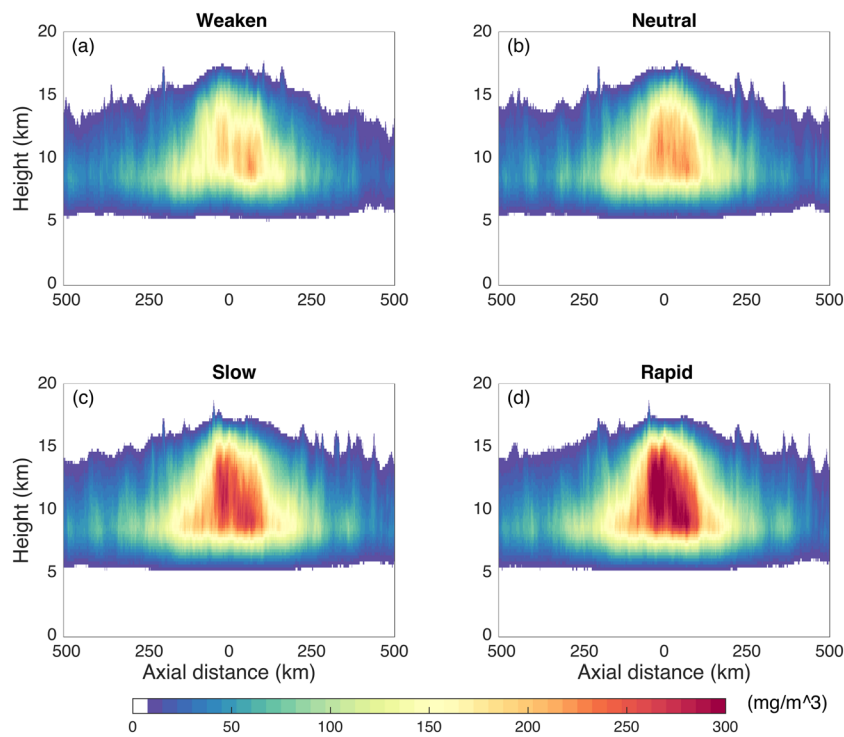


Figure 1. Composites of IWC from CloudSat measurements for (a) weakening, (b) neutral, (c) slowly intensifying, and (d) rapidly intensifying TCs. The *x* axis is the axial distance from the PCA in km and the *y* axis is height in km. Shading is IWC (mg/m^3).

NHC at a grid spacing of 13.5 km and (ii) multiple storm-following nested domains, at grid spacings of 4.5 and 1.5 km, respectively, that deliver high-resolution forecasts for several TCs simultaneously (Alaka et al., 2017). Previous work has shown improvement to TC track and intensity forecasts relative to the operational HWRF (Alaka et al., 2017; Gopalakrishnan et al., 2020). HWRF-B simulations were produced for up to three TCs in the North Atlantic and eastern North Pacific basins in 2018. Forecasts are produced every 6 h with a length of 126 h. Here we focus on the first 72 h of the forecasts for TCs and invests (i.e., tropical systems that are precursors to TCs) in the North Atlantic basin. In total, 499 HWRF-B forecast cycles were evaluated in this study.

3. Results

We create composites of IWC from CloudSat measurements and separate them into four groups based on rates of TC intensification. Figure 1 shows how the distribution and magnitude of IWC are related to rates of TC intensification. The horizontal distribution of IWC is similar across four intensification rates: the maximum is within 100 km of the PCA and the value decreases as one moves outward from the PCA. In terms of the vertical distribution, the largest IWCs are between 8 and 15 km, overlapping with the area of high energy transformation efficiency suggested by Nolan et al. (2007). Meanwhile, the magnitude of IWC varies by group: average IWC becomes greater as the intensification rate increases, and the increase of IWC is distributed mostly within 100 km of the PCA. That being said, the composite for rapidly intensifying TCs has the largest IWC, and is about 70% larger than that for weakening TCs, 50% larger than for neutral TCs, and 15% larger than for slowly intensifying TCs. The area with greater IWC in the composite for rapidly intensifying TCs supports previous studies that identify latent heat release from deep convection as a trigger for rapid intensification (Guimond et al., 2010; Rogers et al., 2013).

In Figure 2, we correlate IWC with intensification rates for every overpass that penetrates TCs within 100 km of the TC center to further quantify the relationship between intensification rates and IWC. Most correlation coefficients above 8 km are positive, especially within 100 km of the PCA, where the values are all positive.

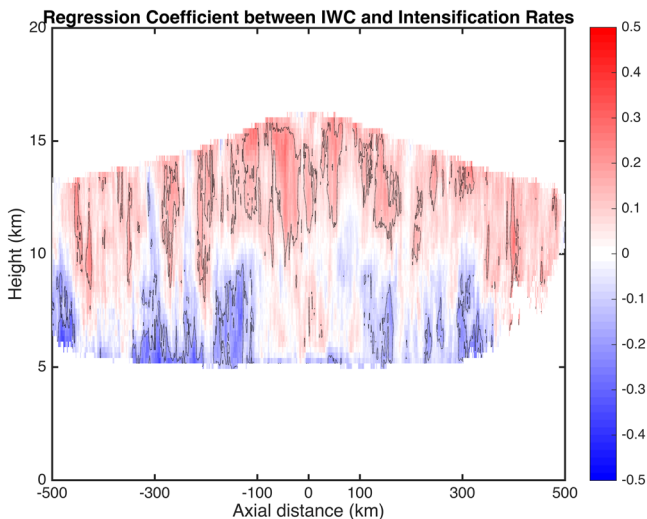


Figure 2. Composites of correlation coefficients between IWC from CloudSat overpasses and rate of TC intensification. The contours indicate regions with a confidence level greater than 95% confidence level. The x axis is the axial distance from the PCA in km, and the y axis is height in km. Shadings are the correlation coefficient of IWC and intensification rate.

This area also overlaps with the region that has the largest magnitude of IWC in the composite for rapidly intensifying TCs (Figure 1). The distribution of positive correlation coefficients has two implications: (1) TCs with greater IWC tend to intensify more quickly in the following 24 h, consistent with previous studies using passive satellite measurements (Fischer et al., 2018; Harnos & Nesbitt, 2016; Jones et al., 2006); (2) with more convective heating, TCs have a greater likelihood to intensify more quickly, according to previous modeling studies that find a high correlation between IWC and latent heat release in the middle-to-upper troposphere (Nolan et al., 2019).

Although most of these correlation coefficients are only around 0.3, these low values may be partly due to the narrow swath of CloudSat measurements (~ 1.4 km). Since convective activity increases as one moves closer to the TC center, CloudSat will tend to observe greater IWC when overpasses are closer to the TC center. Therefore, variations in the distance of the PCA to the TC center will likely introduce noise and diminish the correlation between IWC and the rate of TC intensification. Nevertheless, IWC is still positively correlated with intensification rates in the region where latent heat release is most effective at strengthening TCs, highlighting the potential of IWC measurements to provide information on the evolution of TC intensity in the following 24 h. In addition, we regressed IWC as a function of intensification rates and the distance from

TC center the PCA, as well as intensification rates and TC intensity, respectively. The distribution of regression coefficients is similar to that of correlation coefficients. That is, the greater positive values are concentrated within 100 km of the PCA (supporting information Figures S1 and S2).

In addition to the vertical distribution of cloud ice, we also examine how the horizontal distribution varies with intensification rate. To do this, we calculate ice water path (column integrated IWC; IWP) and create composites as a function of intensification rate for HWRF-B simulations (Figures 3a–3d). Similar to CloudSat, the amount of IWP increases as the intensification rate increases. We further illustrate this relationship between IWP and intensification rate by subtracting the composite for rapidly intensifying TCs from other intensification rates (Figures 3e–3g). The largest difference occurs within 100 km of the TC center. This is consistent with the area of positive correlation coefficients found in CloudSat IWC, suggesting the importance of high-resolution data sets to identify the signal and physical processes of rapid intensification.

TC intensity also influences the amount of IWC in TCs (Cecil & Zipser, 1999; Nolan et al., 2019). That is, stronger TCs tend to generate a greater amount of IWC, as stronger TCs typically have more vigorous convection. Regardless, Fischer et al. (2018) found the dependence of IWP on intensification rates once the effects of TC intensity were accounted for. Therefore, the greater IWC in the composite for rapidly intensifying TCs that we found above may partially reflect the correlation between TC intensity and rates of TC intensification. To address this question, we examine the distribution of TC intensity at the onset of the intensity change window as a function of intensification rates, which are weakening, neutral, slowly intensifying, and rapidly intensifying TCs (Figures S3 and S4). Both best track and HWRF-B showed that TC intensity on average gets stronger as the intensification rate increases, except for weakening TCs. Rapidly intensifying TCs in our data set have the strongest mean TC intensity, indicating that the rapid intensification often occurs when TCs are structurally organized, consistent with previous research (Shapiro & Willoughby, 1982; Vigh et al., 2012). The distribution of TC intensity found here is consistent with a previous study which also demonstrated that rapidly intensifying TCs have the strongest TC intensity among all intensification rates (Hendricks et al., 2010; Knaff et al., 2020).

To exclude the influence of TC intensity on the amount of IWC, we separate CloudSat measurements into three intensity categories (tropical depression, tropical storm, Category 1–3 TC) and then calculate their areal mean IWP within 100 km of the PCA for three intensification rates, respectively (Figure 4). The reason for excluding category 4–5 hurricanes is due to the low occurrence of rapid intensification at this initial intensity category, typically less than 3% (Kaplan et al., 2010). That is, most TCs that experience rapid

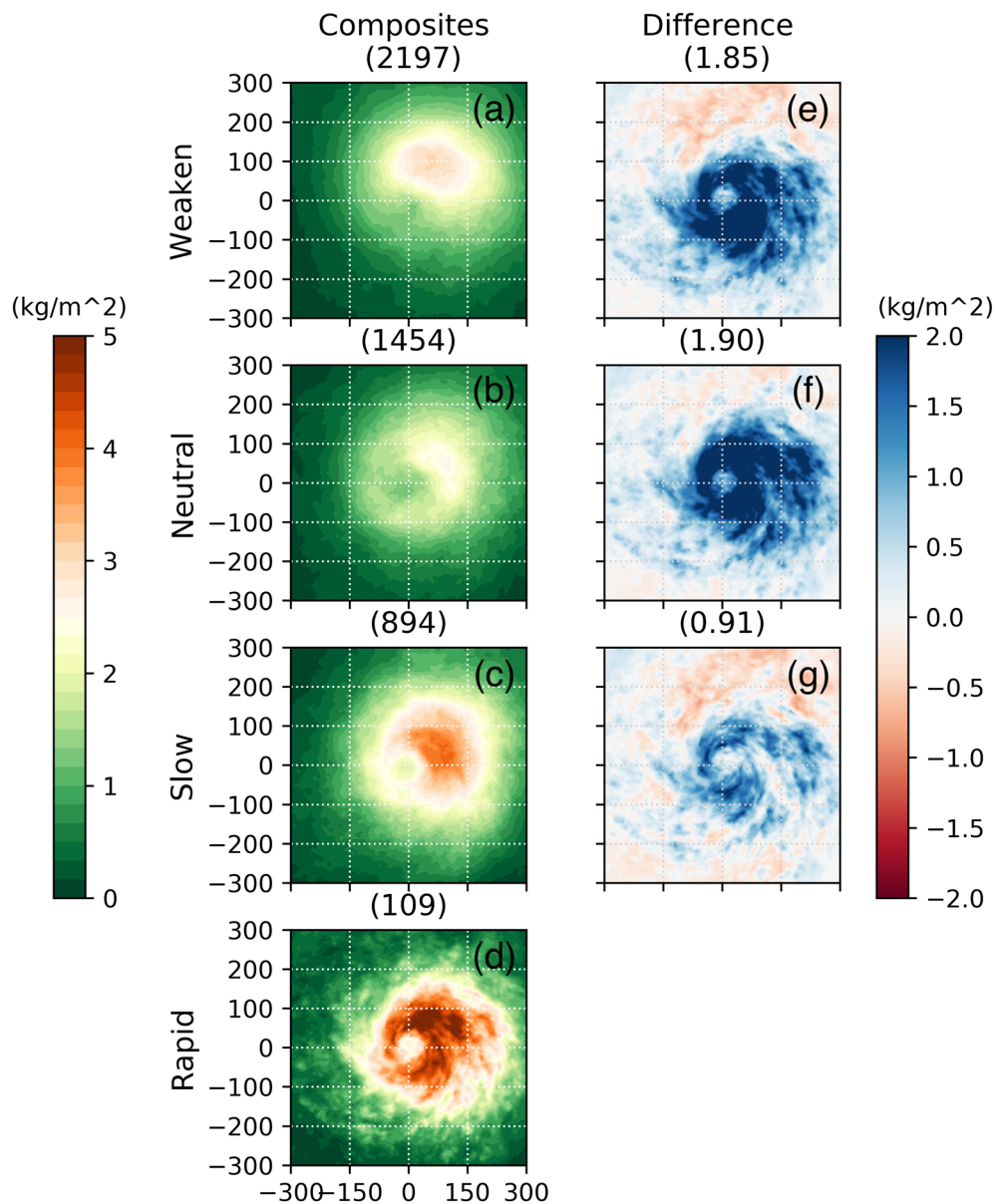


Figure 3. Composites of IWP in HWRF-B for (a) weakening, (b) neutral, (c) slowly intensifying, and (d) rapidly intensifying TCs, and difference in IWP between rapidly intensifying TCs and (e) weakening, (f) neutral, (g) slowly intensifying TCs. Shadings are IWP in kg/m². The x and y axes are the radial distance from the TC center in kilometers. For (a)–(d), the number of cases in each composite is printed above the panel. For (e)–(g), the average IWP difference within 100 km of the TC center is printed above the panel.

intensification in their lifetime grow to category 4–5 hurricane status after rapid intensification, rather than initiating rapid intensification at this category (Kaplan & DeMaria, 2003; Lee et al., 2016). Considering the same intensity category, differences in intensity between four intensification rates are less than 5 kt, except Category 1–3 where the average intensity of rapidly intensifying TCs is 13.2 kt less than slowly intensifying TCs. In this analysis, the mean IWP increases as TC intensity gets stronger, which is consistent with the aforementioned analysis related to IWC and previous studies (Wu & Soden, 2017). Comparing different intensification rates in the same intensity category, the mean IWP becomes greater as the intensification rate increases. That is, rapidly intensifying TCs have the greatest mean IWP among all intensification rates, consistent with previous studies (Fischer et al., 2018; Harnos & Nesbitt, 2016). In addition, we repeated the same analysis for retrievals of IWC from CloudSat of 2C-ICE version, which

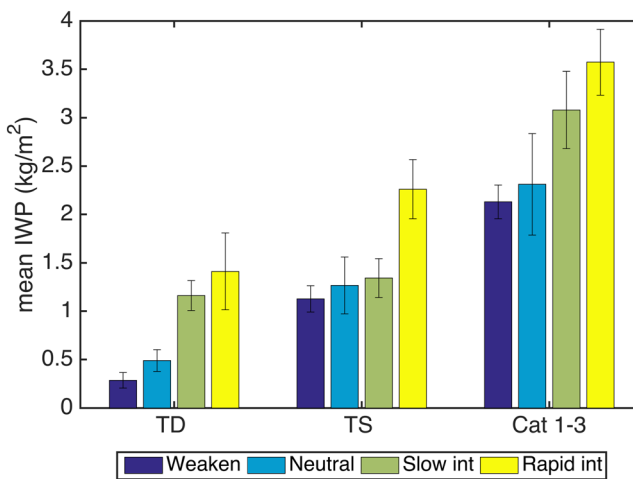


Figure 4. The mean IWP within 100 km of the PCA for four intensification rates in CloudSat: weakening (dark blue), neutral (blue), slowly intensifying (green), and rapidly intensifying (yellow) TCs in three intensity categories (from left to right: tropical depression, tropical storm, Category 1–3 TC), respectively. The y axis is the mean IWP in kg/m². The error bars are one standard error from the mean.

provides a better quality of IWC retrievals. The results associated with 2C-ICE suggested that rapidly intensifying TCs tend to have a greater amount of mean IWP, while the differences between different intensification rates are not as robust because of a limited sample size (Figure S5). The results shown here emphasize the viability of high-resolution, radar-based satellite measurement as forecast guidance for TC rapid intensification.

The same analysis is performed for HWRF-B. For HWRF-B, any 24-h window within 6–72-h forecasts are all separate composites (e.g., 6–30, 12–36, and 18–42). Instead of using the PCA, we calculate the areal mean IWP within 100 km of the TC center (Figure S6). The results are consistent with CloudSat measurements; mean IWP increases as the intensity increases or the intensification rate becomes faster. For all TC intensity categories, the range of IWP ± one standard error does not overlap for weakening, neutral, and intensifying TCs (slowly and rapid combined), indicating a clear distinction in IWP for these intensification rates. For tropical storms and Category 1–2 TCs, the range of IWP ± one standard error also does not overlap for rapidly and slowly intensifying TCs. The consistency between CloudSat and HWRF-B results indicate that IWP from high resolution data sets are able to detect the signal of future rapid intensification.

4. Conclusion

This study examines the signal of rapidly intensifying TCs in high-resolution CloudSat measurements of IWC and HWRF-B simulations of IWP. We found that rapidly intensifying TCs have the largest IWP compared to more slowly intensifying TCs. In addition, IWC is also positively correlated with intensification rates in the area where high energy transformation efficiency possibly occurs (i.e., inside the radius of maximum wind), consistent with theoretical arguments based on numerical models. To minimize the influence of initial intensity on the intensification rates and the amount of observed IWC, CloudSat overpasses and HWRF-B simulations were further separated into three initial intensity categories. These analyses demonstrated that rapidly intensifying TCs still have a greater IWP than other intensification rates, even after accounting for the influence of initial TC intensity. These results show that IWC from the CloudSat profiling radar can serve as a predictor of the onset of TC rapid intensification, consistent with previous studies using microwave satellite measurements. This study further demonstrated that intensification rates are strongly correlated with higher IWC in the upper troposphere, rather than distributed uniformly in the vertical. It also supported previous modeling studies regarding the importance of the spatial distribution of latent heat release in intensifying TCs. More analyses are required to evaluate the skill of numerical models in simulating processes related to RI, and to assess the potential utility of IWC observations in statistical TC models.

Data Availability Statement

CloudSat overpasses were downloaded directly from CloudSat Tropical Cyclone Overpass data set (<https://adelaide.cira.colostate.edu/tc/>). Data are available through Tourville et al. (2015). Best track data are from the NOAA website (<https://www.nhc.noaa.gov/data/>). IBTrACS can be downloaded from the NOAA website (<https://www.ncdc.noaa.gov/ibtracs/>). HWRF-B forecast data are archived on the NOAA Environmental Security Computing Center High Performance Storage System.

Acknowledgments

The authors acknowledge two reviewers whose comments led to substantial improvements of this paper. This work is supported by a grant from the NASA CloudSat/CALIPSO Science Team program. This research was also partially supported by NASA Award 80NSSC18K1032.

References

- Alaka, G. J., Zhang, X., Gopalakrishnan, S. G., Goldenberg, S. B., & Marks, F. D. (2017). Performance of basin-scale HWRF tropical cyclone track forecasts. *Weather and Forecasting*, 32(3), 1253–1271. <https://doi.org/10.1175/WAF-D-16-0150.1>
- Alvey, G. R. III, Zawislak, J., & Zipser, E. (2015). Precipitation properties observed during tropical cyclone intensity change. *Monthly Weather Review*, 143(11), 4476–4492. <https://doi.org/10.1175/MWR-D-15-0065.1>
- Arakawa, A., & Schubert, W. H. (1974). Interaction of a cumulus cloud ensemble with the large-scale environment, Part I. *Journal of the Atmospheric Sciences*, 31(3), 674–701. [https://doi.org/10.1175/1520-0469\(1974\)031<0674:IOACCE>2.0.CO;2](https://doi.org/10.1175/1520-0469(1974)031<0674:IOACCE>2.0.CO;2)
- Atlas, R., Tallapragada, V., & Gopalakrishnan, S. G. (2015). Advances in tropical cyclone intensity forecasts. *Marine Technology Society Journal*, 49(6), 149–160. <https://doi.org/10.4031/MTSJ.49.6.2>

- Bao, J., Gopalakrishnan, S. G., Michelson, S. A., Marks, F. D., & Montgomery, M. T. (2012). Impact of physics representations in the HWRFX on simulated hurricane structure and pressure–wind relationships. *Monthly Weather Review*, 140(10), 3278–3299. <https://doi.org/10.1175/MWR-D-11-00332.1>
- Biswas, M. K., Carson, L., Newman, K., Stark, D., Kalina, E., Grell, E., & Frimel, J. (2018). Community HWRF users' guide V4.0a, 162 pp. https://dtcenter.org/sites/default/files/community-code/hwrf/docs/users_guide/HWRF-UG-2018.pdf
- Cecil, D. J., & Zipser, E. J. (1999). Relationships between tropical cyclone intensity and satellite-based indicators of inner core convection: 85-GHz ice-scattering signature and lightning. *Monthly Weather Review*, 127(1), 103–123. [https://doi.org/10.1175/1520-0493\(1999\)127<0103:RBTCLA>2.0.CO;2](https://doi.org/10.1175/1520-0493(1999)127<0103:RBTCLA>2.0.CO;2)
- Chen, W.-T., Woods, C. P., Li, J.-L. F., Waliser, D. E., Chern, J.-D., Tao, W.-K., et al. (2011). Partitioning CloudSat ice water content for comparison with upper tropospheric ice in global atmospheric models. *Journal of Geophysical Research*, 116(D19), D19206. <https://doi.org/10.1029/2010jd015179>
- DeMaria, M., Sampson, C. R., Knaff, J. A., & Musgrave, K. D. (2014). Is tropical cyclone intensity guidance improving? *Bulletin of the American Meteorological Society*, 95(3), 387–398. <https://doi.org/10.1175/BAMS-D-12-00240.1>
- Elsberry, R. L., Lambert, T. D. B., & Boothe, M. A. (2007). Accuracy of Atlantic and Eastern North Pacific tropical cyclone intensity forecast guidance. *Weather and Forecasting*, 22(4), 747–762. <https://doi.org/10.1175/waf1015.1>
- Ferrier, B. S., Jin, Y., Lin, Y., Black, T., Rogers, E., & DiMego, G. (2002). Implementation of a new grid-scale cloud and precipitation scheme in the NCEP Eta model, 19th Conf. on Weather Analysis and Forecasting/15th Conf. on Numerical Weather Prediction, San Antonio, TX, USA, 2002 August 15, Oral Presentation 10.1. https://ams.confex.com/ams/SLS_WAF_NWP/techprogram/paper_47241.htm
- Fischer, M. S., Tang, B. H., Corbosiero, K. L., & Rozoff, C. M. (2018). Normalized convective characteristics of tropical cyclone rapid intensification events in the North Atlantic and eastern North Pacific. *Monthly Weather Review*, 146(4), 1133–1155. <https://doi.org/10.1175/MWR-D-17-0239.1>
- Gall, R., Franklin, J., Marks, F., Rappaport, E. N., & Toepper, F. (2013). The hurricane forecast improvement project. *Bulletin of the American Meteorological Society*, 94(3), 329–343. <https://doi.org/10.1175/bams-d-12-00071.1>
- Gopalakrishnan, S. G., Goldenberg, S., Quirino, T., Zhang, X., Marks, F., Yeh, K., et al. (2012). Toward improving high-resolution numerical hurricane forecasting: Influence of model horizontal grid resolution, initialization, and physics. *Weather and Forecasting*, 27(3), 647–666. <https://doi.org/10.1175/WAF-D-11-00055.1>
- Gopalakrishnan, S. G., Koch, D., Upadhyay, S., DeMaria, M., Marks, F., Rappaport, E. N. et al. (2020). 2019 HFIP R&D activities summary: Recent results and operational implementation. *NOAA HFIP Tech. Rep.* HFIP2020-1, 42 pp., http://www.hfip.org/documents/HFIP_AnnualReport_FY2019.pdf
- Gopalakrishnan, S. G., Marks, F., Zhang, J. A., Zhang, X., Bao, J., & Tallapragada, V. (2013). A study of the impacts of vertical diffusion on the structure and intensity of the tropical cyclones using the high-resolution HWRF system. *Journal of the Atmospheric Sciences*, 70(2), 524–541. <https://doi.org/10.1175/JAS-D-11-0340.1>
- Gopalakrishnan, S. G., Marks, F., Zhang, X., Bao, J., Yeh, K., & Atlas, R. (2011). The experimental HWRF system: A study on the influence of horizontal resolution on the structure and intensity changes in tropical cyclones using an idealized framework. *Monthly Weather Review*, 139(6), 1762–1784. <https://doi.org/10.1175/2010MWR3535.1>
- Grell, G. A. (1993). Prognostic evaluation of assumptions used by cumulus parameterizations. *Monthly Weather Review*, 121(3), 764–787. [https://doi.org/10.1175/1520-0493\(1993\)121<0764:PEOAUB>2.0.CO;2](https://doi.org/10.1175/1520-0493(1993)121<0764:PEOAUB>2.0.CO;2)
- Guimond, S. R., Heymsfield, G. M., & Turk, F. J. (2010). Multiscale observations of Hurricane Dennis (2005): The effects of hot towers on rapid intensification. *Journal of the Atmospheric Sciences*, 67(3), 633–654. <https://doi.org/10.1175/2009JAS3119.1>
- Hack, J. J., & Schubert, W. H. (1986). Nonlinear response of atmospheric vortices to heating by organized cumulus convection. *Journal of the Atmospheric Sciences*, 43(15), 1559–1573. [https://doi.org/10.1175/1520-0469\(1986\)043<1559:NROAVT>2.0.CO;2](https://doi.org/10.1175/1520-0469(1986)043<1559:NROAVT>2.0.CO;2)
- Harnos, D. S., & Nesbitt, S. W. (2016). Passive microwave quantification of tropical cyclone inner-core cloud populations relative to subsequent intensity change. *Monthly Weather Review*, 144(11), 4461–4482. <https://doi.org/10.1175/MWR-D-15-0090.1>
- Hendricks, E. A., Peng, M. S., Fu, B., & Li, T. (2010). Quantifying environmental control on tropical cyclone intensity change. *Monthly Weather Review*, 138, 3243–3271.
- Iacono, M. J., Delamere, J. S., Mlawer, E. J., Shephard, M. W., Clough, S. A., & Collins, W. D. (2008). Radiative forcing by long-lived greenhouse gases: Calculations with the AER radiative transfer models. *Journal of Geophysical Research*, 113, D13103. <https://doi.org/10.1029/2008JD009944>
- Jones, T. A., Cecil, D., & DeMaria, M. (2006). Passive-microwave-enhanced statistical hurricane intensity prediction scheme. *Weather and Forecasting*, 21(4), 613–635. <https://doi.org/10.1175/WAF941.1>
- Kaplan, J., & DeMaria, M. (2003). Large-scale characteristics of rapidly intensifying tropical cyclones in the North Atlantic Basin. *Weather and Forecasting*, 18(6), 1093–1108. [https://doi.org/10.1175/1520-0434\(2003\)018<1093:LCORIT>2.0.CO;2](https://doi.org/10.1175/1520-0434(2003)018<1093:LCORIT>2.0.CO;2)
- Kaplan, J., DeMaria, M., & Knaff, J. A. (2010). A revised tropical cyclone rapid intensification index for the Atlantic and Eastern North Pacific Basins. *Weather and Forecasting*, 25(1), 220–241. <https://doi.org/10.1175/2009waf2222280.1>
- Kelley, O. A., Stout, J., & Halverson, J. B. (2004). Tall precipitation cells in tropical cyclones eyewalls are associated with tropical cyclone intensification. *Geophysical Research Letters*, 31, L24112. <https://doi.org/10.1029/2004GL021616>
- Knaff, J. A., Sampson, C. R., & DeMaria, M. (2005). An operational statistical typhoon intensity prediction scheme for the Western North Pacific. *Weather and Forecasting*, 20(4), 688–699. <https://doi.org/10.1175/WAF863.1>
- Knaff, J. A., Sampson, C. R., & Strahl, B. R. (2020). A tropical cyclone rapid intensification prediction aid for the Joint Typhoon Warning Center's areas of responsibility. *Weather and Forecasting*, 35(3), 1173–1185. <https://doi.org/10.1175/WAF-D-19-0228.1>
- Knapp, K. R., Diamond, H. J., Kossin, J. P., Kruk, M. C., & Schreck, C. J. (2018). International best track archive for climate stewardship (IBTrACS) project, version 4. [indicate subset used]. NOAA National Centers for Environmental Information. Non-government domain. <https://doi.org/10.25921/82ty-9e16> [access date].
- Lee, C.-Y., Tippett, M. K., Sobel, A. H., & Camargo, S. J. (2016). Rapid intensification and the bimodal distribution of tropical cyclone intensity. *Nature Communications*, 7(1), 10625. <https://doi.org/10.1038/ncomms10625>
- Lewis, W. E., Velden, C. S., & Stettner, D. (2020). Strategies for assimilating high-density atmospheric motion vectors into a regional tropical cyclone forecast model (HWRF). *Atmosphere*, 11, 673.
- Mehra, A., Tallapragada, V., Zhang, Z., Liu, B., Zhu, L., Wang, W., & Kim, H.-S. (2018). Advancing the state of the art in operational tropical cyclone forecasting at NCEP. *Tropical Cyclone Research and Review*, 7, 51–56. <https://doi.org/10.6057/2018TCRR01.06>
- Mlawer, E., Taubman, S., Brown, P., Iacono, M., & Clough, S. (1997). Radiative transfer for inhomogeneous atmosphere: RRMT, a validated correlated-k model for the longwave. *Journal of Geophysical Research*, 102(D14), 16,663–16,682. <https://doi.org/10.1029/97JD00237>

- Nolan, D. S., Miyamoto, Y., Wu, S., & Soden, B. J. (2019). On the correlation between total condensate and moist heating in tropical cyclones and applications for diagnosing intensity. *Monthly Weather Review*, 147(10), 3759–3784. <https://doi.org/10.1175/MWR-D-19-0010.1>
- Nolan, D. S., Moon, Y., & Stern, D. P. (2007). Tropical cyclone intensification from asymmetric convection: Energetics and efficiency. *Journal of the Atmospheric Sciences*, 64(10), 3377–3405. <https://doi.org/10.1175/JAS3988.1>
- Pan, H. L., & Wu, J. (1995). Implementing a mass flux convection parameterization package for the NMC medium-range forecast model. *NMC Office Note No. 409*, 40 pp., <https://repository.library.noaa.gov/view/noaa/11429>
- Rogers, E., Black, T., Ferrier, B., Lin, Y., Parrish, D., & DiMego, G. (2001). NCEP Meso Eta Analysis and Forecast System: Increase in resolution, new cloud microphysics, modified precipitation assimilation, modified 3DVAR analysis. *NWS Technical Procedures Bulletin*, 488, 1–15.
- Rogers, R., Reasor, P., & Lorsolo, S. (2013). Airborne Doppler observations of the inner-core structural differences between intensifying and steady-state tropical cyclones. *Monthly Weather Review*, 141(9), 2970–2991. <https://doi.org/10.1175/MWR-D-12-00357.1>
- Shapiro, L. J., & Willoughby, H. E. (1982). The response of balanced hurricanes to local sources of heat and momentum. *Journal of the Atmospheric Sciences*, 39(2), 378–394. [https://doi.org/10.1175/1520-0469\(1982\)039<0378:TROBHT>2.0.CO;2](https://doi.org/10.1175/1520-0469(1982)039<0378:TROBHT>2.0.CO;2)
- Shimada, U., Owada, H., Yamaguchi, M., Iriuchi, T., Sawada, M., Aonashi, K., et al. (2018). Further improvements to the statistical hurricane intensity prediction scheme using tropical cyclone rainfall and structural features. *Weather and Forecasting*, 33(6), 1587–1603. <https://doi.org/10.1175/WAF-D-18-0021.1>
- Simon, A., Penny, A. B., DeMaria, M., Franklin, J. L., Pasch, R. J., Rappaport, E. N., & Zelinsky, D. A. (2018). A description of the real-time HFIP corrected consensus approach (HCCA) for tropical cyclone track and intensity guidance. *Weather and Forecasting*, 33(1), 37–57. <https://doi.org/10.1175/WAF-D-17-0068.1>
- Stephens, G. L., Vane, D. G., Boain, R. J., Mace, G. G., Sassen, K., Wang, Z., et al. (2002). The CloudSat mission and the A-Train. *Bulletin of the American Meteorological Society*, 83, 1771–1790.
- Tallapragada, V., Kieu, C., Kwon, Y., Trahan, S., Liu, Q., Zhang, Z., & Kwon, I. (2014). Evaluation of storm structure from the operational HWRF during 2012 implementation. *Monthly Weather Review*, 142(11), 4308–4325. <https://doi.org/10.1175/MWR-D-13-00010.1>
- Tao, C., & Jiang, H. (2015). Distributions of shallow to very deep precipitation-convection in rapidly intensifying tropical cyclones. *Journal of Climate*, 28(22), 8791–8824. <https://doi.org/10.1175/JCLI-D-14-00448.1>
- Tao, C., Jiang, H., & Zawislak, J. (2017). The relative importance of stratiform and convective rainfall in rapidly intensifying tropical cyclones. *Monthly Weather Review*, 145(3), 795–809. <https://doi.org/10.1175/MWR-D-16-0316.1>
- Tourville, N., Stephens, G., DeMaria, M., & Vane, D. (2015). Remote sensing of tropical cyclones: Observations from CloudSat and A-Train profilers. *Bulletin of the American Meteorological Society*, 96(4), 609–622. <https://doi.org/10.1175/BAMS-D-13-00282.1>
- Vigh, J. L., Knaff, J. A., & Schubert, W. H. (2012). A climatology of hurricane eye formation. *Monthly Weather Review*, 140(5), 1405–1426. <https://doi.org/10.1175/MWR-D-11-00108.1>
- Waliser, D. E., Li, J. L., Woods, C. P., Austin, R. T., Bacmeister, J., Chern, J., et al. (2009). Cloud ice: A climate model challenge with signs and expectations of progress. *Journal of Geophysical Research*, 114, D00A21. <https://doi.org/10.1029/2008JD010015>
- Wu, S., & Soden, B. J. (2017). Signatures of tropical cyclone intensification in satellite measurements of ice and liquid water content. *Monthly Weather Review*, 145(10), 4081–4091. <https://doi.org/10.1175/MWR-D-17-0046.1>
- Yanai, M., Esbensen, S., & Chu, J.-H. (1973). Determination of bulk properties of tropical cloud clusters from large-scale heat and moisture budgets. *Journal of the Atmospheric Sciences*, 30(4), 611–627. [https://doi.org/10.1175/1520-0469\(1973\)030<0611:dbpot>2.0.co;2](https://doi.org/10.1175/1520-0469(1973)030<0611:dbpot>2.0.co;2)
- Zagrodnik, J. P., & Jiang, H. (2014). Rainfall, convection, and latent heating distributions in rapidly intensifying tropical cyclones. *Journal of the Atmospheric Sciences*, 71(8), 2789–2809. <https://doi.org/10.1175/JAS-D-13-0314.1>
- Zhang, X., Gopalakrishnan, S. G., Trahan, S., Quirino, T. S., Liu, Q., Zhang, Z., et al. (2016). Representing multiple scales in the hurricane weather research and forecasting modeling system: Design of multiple sets of movable multilevel nesting and the basin-scale HWRF forecast application. *Weather and Forecasting*, 31(6), 2019–2034. <https://doi.org/10.1175/WAF-D-16-0087.1>